LETTER

doi:10.1038/nature09755

The RAG2 C terminus suppresses genomic instability and lymphomagenesis

Ludovic Deriano[1], Julie Chaumeil[1], Marc Coussens[1], Asha Multani[2], YiFan Chou[1], Alexander V. Alekseyenko[3], Sandy Chang[4], Jane A. Skok[1,5] & David B. Roth[1]

Misrepair of DNA double-strand breaks produced by the V(D)J recombinase (the RAG1/RAG2 proteins) at immunoglobulin (Ig) and T cell receptor (Tcr) loci has been implicated in pathogenesis of lymphoid malignancies in humans[1] and in mice[2–7]. Defects in DNA damage response factors such as ataxia telangiectasia mutated (ATM) protein and combined deficiencies in classical non-homologous end joining and p53 predispose to RAG-initiated genomic rearrangements and lymphomagenesis[2–11]. Although we showed previously that RAG1/RAG2 shepherd the broken DNA ends to classical non-homologous end joining for proper repair[12,13], roles for the RAG proteins in preserving genomic stability remain poorly defined. Here we show that the RAG2 carboxy (C) terminus, although dispensable for recombination[14,15], is critical for maintaining genomic stability. Thymocytes from '*core*' *Rag2* homozygotes (*Rag2*$^{c/c}$ mice) show dramatic disruption of *Tcrα/δ* locus integrity. Furthermore, all *Rag2*$^{c/c}$ *p53*$^{-/-}$ mice, unlike *Rag1*$^{c/c}$ *p53*$^{-/-}$ and *p53*$^{-/-}$ animals, rapidly develop thymic lymphomas bearing complex chromosomal translocations, amplifications and deletions involving the *Tcrα/δ* and *Igh* loci. We also find these features in lymphomas from *Atm*$^{-/-}$ mice. We show that, like ATM-deficiency[3], core RAG2 severely destabilizes the RAG post-cleavage complex. These results reveal a novel genome guardian role for RAG2 and suggest that similar 'end release/end persistence' mechanisms underlie genomic instability and lymphomagenesis in *Rag2*$^{c/c}$ *p53*$^{-/-}$ and *Atm*$^{-/-}$ mice.

RAG mutations can cause specific defects in the joining stage of V(D)J recombination[12,13,16]. The 'dispensable' RAG2 C terminus (murine amino acids 1–383) is of particular interest: loss of the RAG2 C terminus impairs joining of substrates[17], increases levels of double-strand breaks[17] that persist through the cell cycle[18], and increases accessibility of the broken DNA ends to alternative non-homologous end joining[12,19]. Despite these defects, *Rag2*$^{c/c}$ mice are not lymphoma-prone.

We reasoned that *Rag2*$^{c/c}$ *p53*$^{-/-}$ double-mutant mice might display genomic instability and lymphomagenesis, even in the context of intact classical non-homologous end joining. Consistent with previous reports[15], our *Rag2*$^{c/c}$ mice displayed partial developmental blocks in B and T lymphopoiesis because of a selective V-to-DJ rearrangement defect (Supplementary Fig. 1). *Rag2*$^{c/c}$ animals, observed for up to 1 year, showed no obvious signs of tumorigenesis (Fig. 1a and data not shown). As expected[20], approximately two-thirds of *p53*$^{-/-}$ mice developed thymic lymphoma at an average age of approximately 23 weeks (mean survival = 22.8 weeks) (Fig. 1a, b). Similar findings in RAG/p53-deficient mice[21] demonstrate that RAG-initiated double-strand breaks are not critical initiators of lymphomagenesis in p53-deficient mice. In sharp contrast, 100% ($n = 25$) of our *Rag2*$^{c/c}$ *p53*$^{-/-}$ mice died within 16 weeks (mean survival = 12.1 weeks) with aggressive thymic lymphomas (Fig. 1a–c). Tumour cells were highly proliferative and expressed cell surface CD4 and CD8 (Supplementary Fig. 2), with little or no surface TCR (CD3ε or TCRβ) (data not shown), indicating that these tumours originate from immature thymocytes. Tumours with highly proliferating lymphoblasts were detected in 4- to 6-week-old *Rag2*$^{c/c}$ *p53*$^{-/-}$ thymi, but not in other organs (data not shown), confirming their thymic origin. *Rag2*$^{c/c}$ *p53*$^{-/-}$ tumours generally displayed one or a few predominant Dβ1–Jβ1 or Dβ2–Jβ2 rearrangements, indicating a clonal or oligoclonal origin (Supplementary Fig. 3).

We next examined genomic stability in lymphomas from *Rag2*$^{c/c}$ *p53*$^{-/-}$ mice, first by analysis of Giemsa-stained metaphase spreads prepared from 12 *Rag2*$^{c/c}$ *p53*$^{-/-}$ and two *p53*$^{-/-}$ thymic lymphomas (Supplementary Table 1). Wild-type thymocytes showed almost no abnormal metaphases (0–3%) (Supplementary Table 1). In contrast, *p53*$^{-/-}$ and *Rag2*$^{c/c}$ *p53*$^{-/-}$ tumours harboured a variety of cytogenetic aberrations (aberrant metaphases: 8–94%), including aneuploidy, chromosome breaks and chromosome fusions (Supplementary Table 1). We

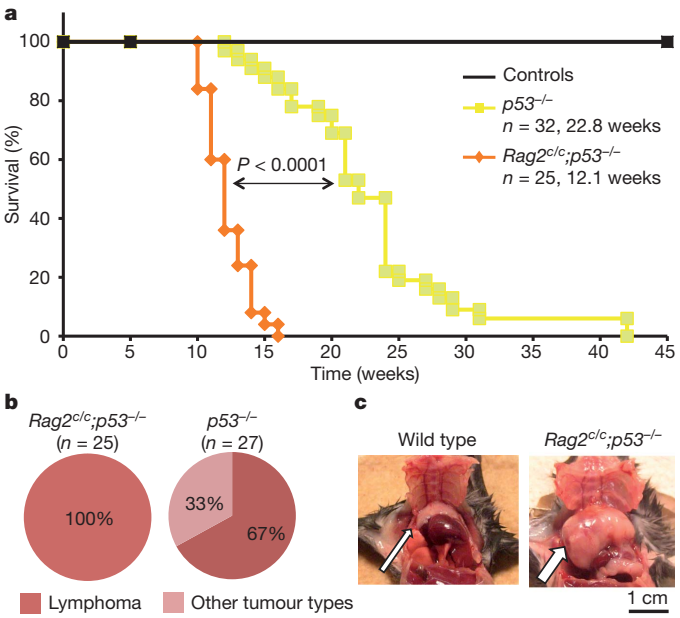

Figure 1 | The C terminus of RAG2 is a tumour suppressor in developing thymocytes. **a**, Kaplan–Meier tumour-free survival analysis for cohorts of control (wild type, $n = 12$; *Rag2*$^{c/c}$, $n = 19$), *p53*$^{-/-}$ ($n = 32$) and *Rag2*$^{c/c}$ *p53*$^{-/-}$ ($n = 25$) mice. Animals were monitored for 50 weeks. The average age of death in weeks is shown for *p53*$^{-/-}$ (22.8 weeks) and *Rag2*$^{c/c}$ *p53*$^{-/-}$ (12.1 weeks) genotypes with the *P* value determined by a Wilcoxon rank sum test. **b**, Tumour spectrum observed for *Rag2*$^{c/c}$ *p53*$^{-/-}$ ($n = 25$) and *p53*$^{-/-}$ mice ($n = 27$). All *Rag2*$^{c/c}$ *p53*$^{-/-}$ animals ($n = 25$) showed enlarged thymus. *p53*$^{-/-}$ animals showed either enlarged thymus and/or spleen ($n = 18$) or other non-lymphoid tumour mass ($n = 9$). **c**, Physical appearance of normal thymus (wild type) and thymic lymphoma (*Rag2*$^{c/c}$ *p53*$^{-/-}$, arrow) of 3-month-old animals.

[1]Department of Pathology, New York University School of Medicine, New York, NY 10016, USA. [2]Department of Genetics, The M.D. Anderson Cancer Center, Houston, TX 77030, USA. [3]Department of Medicine, Division of Clinical Pharmacology, Center for Health Informatics and Bioinformatics, New York University School of Medicine, NY 10016, USA. [4]Department of Laboratory Medicine, Yale University School of Medicine, New Haven, CT 06520, USA. [5]Department of Immunology and Molecular Pathology, Division of Infection and Immunity, University College London, London W1T 4JF, UK.

analysed three *Rag2*$^{c/c}$ *p53*$^{-/-}$ thymic lymphomas using spectral (1790T and 1745T) and G-band (1779T) karyotyping (Fig. 2). We observed recurrent translocations involving chromosomes that harbour *Tcr* (chromosomes 14 and 6) and *Ig* (chromosomes 12, 6 and 16) loci, suggesting that these might have been initiated by RAG-generated breaks. Moreover, all three lymphomas harboured translocations of the *Igh* locus-containing chromosome 12 and/or the *Tcrα/δ* locus-containing chromosome 14, loci that rearrange in thymocytes[22]. Analysis of lymphoma 1779T revealed a C12;14 translocation (Fig. 2). These results suggest that *Rag2*$^{c/c}$ *p53*$^{-/-}$ T cell tumours harbour clonal translocations involving the *Tcrα/δ* and *Igh* loci, as seen in T-cell lymphomas from patients with ataxia–telangiectasia and *Atm*$^{-/-}$ mice[7,8,10,11], rearrangements not observed in *p53*$^{-/-}$ lymphomas[21,23].

To confirm the involvement of the *Tcrα/δ* locus in chromosome translocations, we performed DNA fluorescence *in situ* hybridization (DNA FISH) analyses on metaphases from *Rag2*$^{c/c}$ *p53*$^{-/-}$ thymic lymphomas (2489T and 2805T) using probes centromeric (*Tcrα/δ V*) and telomeric (*Tcrα/δ C*) to the *Tcrα/δ* locus plus a paint for chromosome 14 (Fig. 3a). In both tumours, breakpoints within the *Tcrα/δ* locus of one of the two chromosomes 14 resulted in amplification of the *Tcrα/δ V* region (Fig. 3a). The telomeric fragment (including *Tcrα/δ C*) was either translocated (2489T), or lost (2805T) (Fig. 3a). DNA FISH analysis of tumours 1790T and 1779T (from Fig. 2) using *Tcrα/δ C* and *V* probes also confirmed translocation of chromosome 14 with breakpoints within the *Tcrα/δ* locus, although without obvious amplification (Supplementary Fig. 4).

We next performed DNA FISH on *Rag2*$^{c/c}$ *p53*$^{-/-}$ thymic lymphomas 2489T and 2805T using probes centromeric (*Igh C*) and telomeric (*Igh V*) to the *Igh* locus along with a chromosome 12 paint (Fig. 3b). In both lymphomas, one chromosome 12 showed translocation with another chromosome, with accompanying loss of both *Igh C* and *V* signals (Fig. 3b). This could result from RAG-induced breaks with loss of the telomeric end of the chromosome (including *Igh V*) and loss of the *Igh C* region by end degradation before fusion to the partner chromosome, as previously reported in *Atm*$^{-/-}$ mouse T cells[8]. Moreover, dual chromosome 12 and 14 paint analysis showed a C12;14 translocation in lymphoma 2489T (Fig. 3b). In contrast to *Rag2*$^{c/c}$ *p53*$^{-/-}$ lymphomas, DNA FISH on metaphases from one *p53*$^{-/-}$ thymic lymphoma (6960T) indicated that both *Tcrα/δ* and *Igh* loci were intact (Supplementary Fig. 5), consistent with previous work[21].

We next performed array-based comparative genomic hybridization (a-CGH) analysis on genomic DNA from five *Rag2*$^{c/c}$ *p53*$^{-/-}$ thymic lymphomas (2489T, 2805T, 1348T, 1779T, 1780T). We observed loss or gain of a region within the *Tcrα/δ* and *Igh* loci, reflecting V(D)J recombination (Supplementary Fig. 6). All five *Rag2*$^{c/c}$ *p53*$^{-/-}$ lymphomas examined showed substantial amplification of a common region on chromosome 14, centromeric of the *Tcrα/δ* locus (Supplementary Fig. 6a), in agreement with our FISH analyses (Fig. 3a). We also observed loss of a common region on chromosome 12, telomeric of the *Igh* locus in all five *Rag2*$^{c/c}$ *p53*$^{-/-}$ thymic lymphomas analysed (Supplementary Fig. 6b). Tumours 1779T, 2489T and 2805 also showed loss of a large region centromeric of the *Igh* locus, probably reflecting DNA-end degradation before fusion to the partner chromosome (Figs 2 and 3a, b and Supplementary Fig. 6b). In contrast, aCGH analysis of *p53*$^{-/-}$ thymic lymphoma 6960T failed to reveal amplification centromeric to the *Tcrα/δ* locus or deletion telomeric to the *Igh* locus (Supplementary Fig. 7a, b), in agreement with our FISH analysis (Supplementary Fig. 5) and previous data[23].

Blocking lymphocyte development in early stages can lead to persistent RAG activity, which, in the absence of p53, can provoke lymphomagenesis[23]. To investigate whether the partial developmental block in *Rag2*$^{c/c}$ thymocytes[15] is sufficient to produce genomic instability and lymphomagenesis, we crossed *core Rag1* knock-in animals, which display diminished recombination and a strong block in B- and T-cell development[14,24] (Supplementary Fig. 1), into a p53-deficient background. *Rag1*$^{c/c}$ *p53*$^{-/-}$ mice survived at an average age of 18.7 weeks (Supplementary Fig. 8a), barely distinguishable from *p53*$^{-/-}$ mice. Also like *p53*$^{-/-}$ mice, only two-thirds of *Rag1*$^{c/c}$ *p53*$^{-/-}$ mice developed thymic lymphomas (Supplementary Fig. 8b).

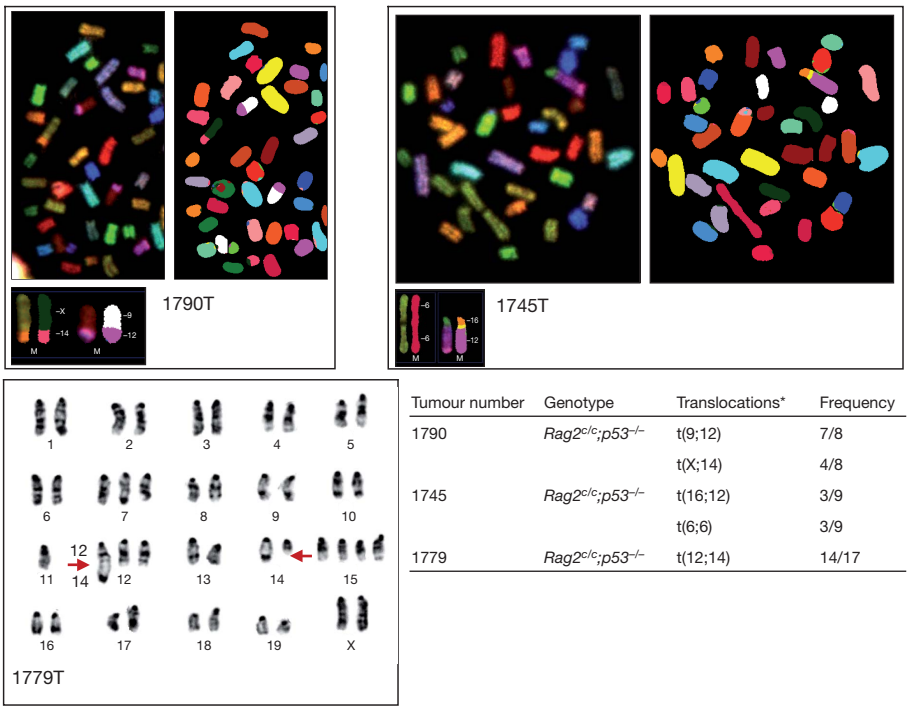

Tumour number	Genotype	Translocations*	Frequency
1790	*Rag2*$^{c/c}$;*p53*$^{-/-}$	t(9;12)	7/8
		t(X;14)	4/8
1745	*Rag2*$^{c/c}$;*p53*$^{-/-}$	t(16;12)	3/9
		t(6;6)	3/9
1779	*Rag2*$^{c/c}$;*p53*$^{-/-}$	t(12;14)	14/17

Figure 2 | *Rag2*$^{c/c}$ *p53*$^{-/-}$ thymic lymphomas display recurrent translocations involving chromosomes that harbour antigen-receptor loci. Representative images of spectral karyotyping (1790T and 1745T) and G-band karyotyping (1779T) analysis of three *Rag2*$^{c/c}$ *p53*$^{-/-}$ T cell lymphomas. Metaphase number analysed and translocations for each tumour sample are listed in the table. All three tumours harbour clonal translocations involving chromosomes that carry *Tcr* (chromosome 14, *Tcrα/δ*; chromosome 6, *Tcrβ*) and/or *Ig* (chromosome 12, *Igh*; chromosome 6, *Igκ*; chromosome 16, *Igλ*) loci.

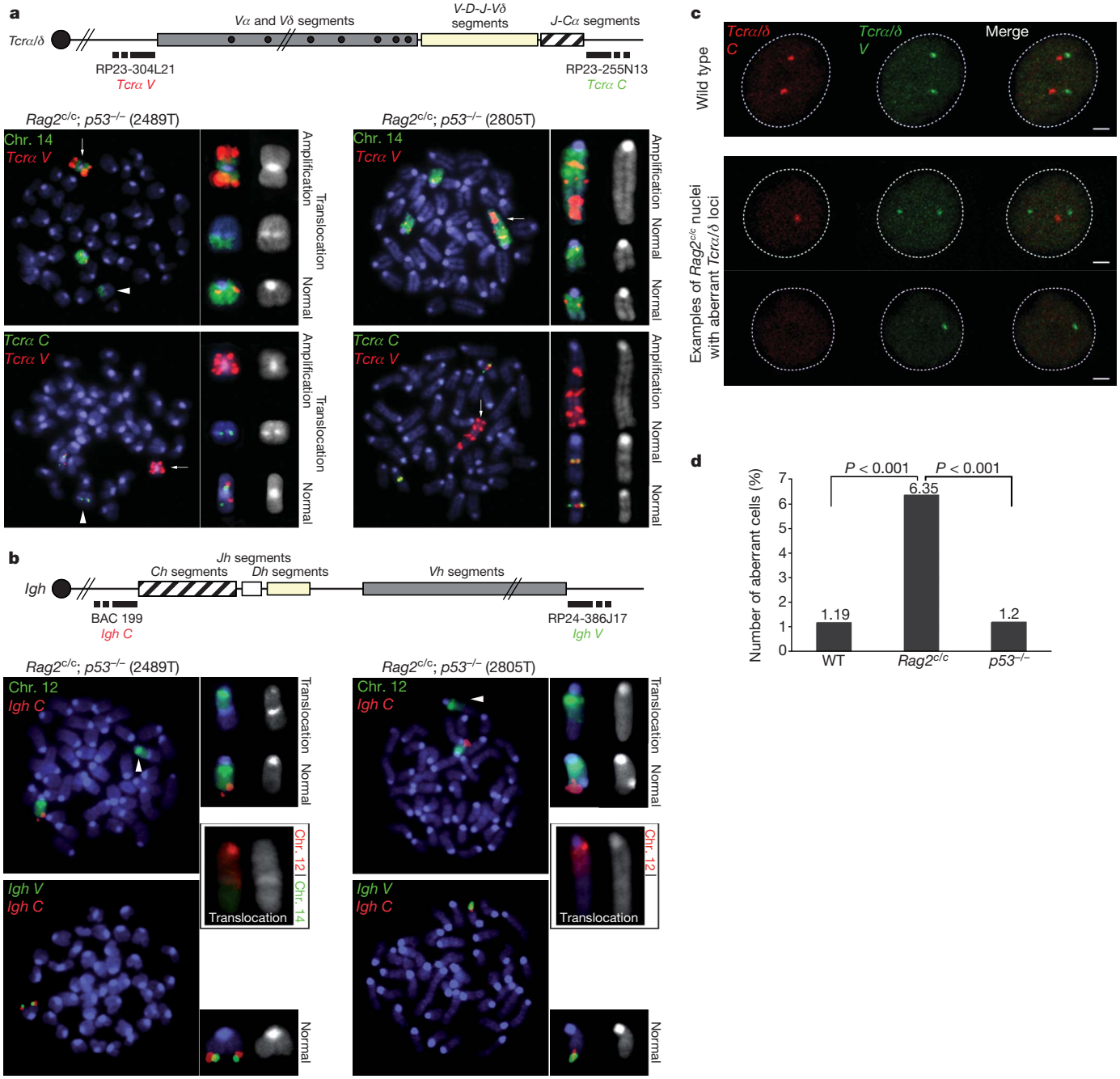

Figure 3 | *Rag2*$^{c/c}$ *p53*$^{-/-}$ thymocytes display *Tcrα/δ*- and *Igh*-associated genomic instability. **a**, Top panel: schematic of the *Tcrα/δ* locus, with positions of the BACs used for generation of DNA FISH probes indicated. Bottom panels: representative metaphases from two *Rag2*$^{c/c}$ *p53*$^{-/-}$ thymic lymphomas using the *Tcrα/δ V* BAC probe (red signal) combined with chromosome 14 paint (green signal, top row) or with the *Tcrα/δ C* BAC probe (green signal, bottom row). Arrows point to the amplification of the *Tcrα/δ V* region, arrowheads point to the translocated chromosome 14. **b**, Top panel: schematic of the *Igh* locus, with positions of the BACs used for generation of DNA FISH probes indicated. Bottom panels: representative metaphases from the same two *Rag2*$^{c/c}$ *p53*$^{-/-}$ thymic lymphomas using the *Igh C* BAC probe (red signal) combined with chromosome 12 paint (green signal, top row) or with the *Igh V* BAC probe (green signal, bottom row). Combination of chromosome 12 (red) and chromosome 14 (green) paints is shown for both tumours in black boxes. Arrowheads point to the translocated chromosome 12. **c**, Examples of confocal sections of three-dimensional *Tcrα/δ* DNA FISH on freshly isolated wild-type (top row) or *Rag2*$^{c/c}$ (bottom rows) double-positive thymocytes. *Tcrα/δ V* (green) and *C* (red) BAC probes were used. Scale bar, 1 μm. **d**, Representative experiment showing the frequency at which *Tcrα/δ V* and/or *Tcrα/δ C* signals are lost in wild-type (WT), *p53*$^{-/-}$ and *Rag2*$^{c/c}$ thymocytes ($n > 200$; see Supplementary Fig. 11 for additional experiments and statistical analysis).

Furthermore, metaphase DNA FISH analyses on two *Rag1*$^{c/c}$ *p53*$^{-/-}$ thymic lymphomas (8383T and 8411T) (Supplementary Fig. 9) and aCGH analysis on genomic DNA from four *Rag1*$^{c/c}$ *p53*$^{-/-}$ thymic lymphomas (8315T, 8333T, 8383T, 8411T) (Supplementary Fig. 10) showed no evidence of recurrent translocations, genomic amplification or genomic deletion at chromosome 14 and chromosome 12. The genomic instability observed in *Rag2*$^{c/c}$ *p53*$^{-/-}$ thymic lymphomas is therefore associated specifically with loss of the RAG2 C terminus, and does not result from the developmental block in *core RAG2* homozygotes.

We next asked whether core RAG2 promotes genomic instability in the presence of p53 by using three-dimensional interphase DNA FISH to examine the integrity of *Tcrα/δ* locus (Fig. 3c) in *Rag2*$^{c/c}$ double-positive thymocytes. The two alleles appeared as two pairs of signals (*Tcrα/δ V* and *Tcrα/δ C*, mapping the two ends of the locus) in most

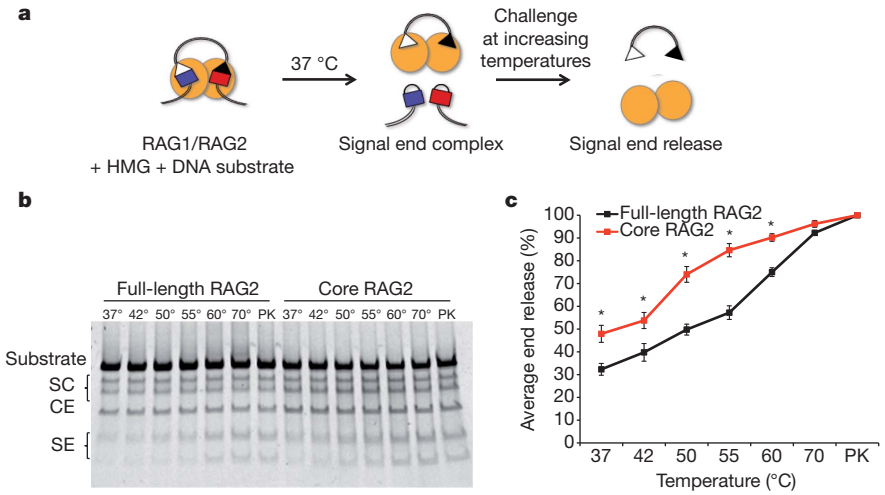

Figure 4 | The C terminus of RAG2 stabilizes the RAG post-cleavage complex. **a**, Biochemical end-release assay. Purified glutathione *S*-transferase (GST)-tagged core RAG1 and non-tagged RAG2 (full length or core) proteins (yellow circles) cleave a 500 base pair (bp) DNA substrate at 37 °C. Post-cleavage signal end complexes are thermally challenged at increasing temperatures to force the release of signal ends, which are detected after electrophoresis and gel staining. **b**, Representative gel for end-release assays. Numbers above each lane indicate the temperatures (in degrees Celsius) the reactions were heated to before electrophoresis. CE, coding ends; SC, single cleavages; PK, samples treated with proteinase K and SDS. **c**, Quantification of signal end release, measured as the combined amount of signal ends divided by the signal from the total amount of DNA in the lane, from six experiments using two different protein preparations (*$P < 0.05$, Student's *t*-test).

(>98%) wild-type and *p53*$^{-/-}$ double-positive thymocytes (Fig. 3d and Supplementary Fig. 11), indicating that p53 deficiency alone does not disrupt the integrity of the *Tcrα/δ* locus, as expected[25]. In contrast, *Rag2*$^{c/c}$ double-positive thymocytes displayed a three- to fivefold increase in the number of cells showing loss of at least one signal (Fig. 3c, d and Supplementary Fig. 11). These results suggest that core RAG2 promotes genomic instability at the *Tcrα/δ* locus, a phenotype similar to that previously reported in *Atm*$^{-/-}$ and *53bp1*$^{-/-}$ animals[9,25].

We noted that both *Rag2*$^{c/c}$ *p53*$^{-/-}$ and *Atm* $^{-/-}$ mice feature RAG-dependent genomic instability at the *Tcrα/δ* and *Igh* loci, with development of pro-T cell lymphomas bearing clonal translocations, including 12/14 translocations[2,3,7–11]. To determine whether *Atm*$^{-/-}$ thymic lymphomas also harbour amplification close to the *Tcrα/δ* locus, we performed DNA FISH analysis for *Tcrα/δ* and chromosome 14 on metaphases from one *Atm*$^{-/-}$ thymic lymphoma (10375T) (Supplementary Fig. 12a). Both chromosomes 14 showed translocations with breakpoints within the *Tcrα/δ* locus, and amplification of the *Tcrα/δ V* region on one allele (Supplementary Fig. 12a), results that were confirmed by aCGH analysis (Supplementary Fig. 12b). We also observed loss of DNA at a distal region of chromosome 12, near the *Igh* locus (Supplementary Fig. 12b), as in *Rag2*$^{c/c}$ *p53*$^{-/-}$ lymphomas (Fig. 3 a, b and Supplementary Fig. 6). These data agree with recent analysis of thymic lymphomas from ATM-deficient mice[7]. Thymic lymphomas that arise in other mutant backgrounds such as p53, core RAG1/p53 (Supplementary Figs 8–10), Eβ/p53 or H2AX/p53 lack recurrent amplifications of chromosome 14 regions and/or recurrent chromosome 12/14 translocations, and thus appear to arise from distinct mechanisms.

Our data reveal a novel *in vivo* function for the RAG2 C terminus in promoting genomic stability. How does core RAG2 allow genomic instability? We hypothesized that core RAG2, like the absence of ATM[3], destabilizes the post-cleavage complex. To investigate this, we generated RAG-signal end complexes by *in vitro* cleavage and challenged them at increasing temperatures, followed by gel electrophoresis (Fig. 4). Complexes containing full-length RAG2 did not release 50% of signal ends until 55 °C (Fig. 4b, c), as expected[13,26]. In contrast, core RAG2-containing complexes displayed statistically significant instability at lower temperatures, with 50% end release at 37 °C (Fig. 4b, c). To examine the post-cleavage complex *in vivo*, we analysed inversional recombination, which requires coordination of all four DNA ends. Decreased inversional recombination and increased formation of hybrid joints (generated by joining of a coding end to a signal end, in this case revealing defects in formation of four-ended inversion products) has been reported in ATM- and MRE11 complex-deficient cells[3,27,28]. As expected[3,28], we observed increased hybrid joint formation at the *Igκ* locus (*Vκ6-23* to *Jκ1*) in *Atm*$^{-/-}$ and *Nbs*$^{\Delta B/\Delta B}$ splenocytes (Supplementary Fig. 13). Importantly, we observed increased *Vκ6-23*-to-*Jκ1* hybrid joints in *Rag2*$^{c/c}$ splenocytes, compared with their wild-type and *Rag2*$^{c/+}$ counterparts (Supplementary Fig. 13). These results are supported by the observation that *Rag2*$^{c/c}$ lymphocytes exhibit defects in inversional recombination[15]. Together, these data support our hypothesis that core RAG2 impairs the stability of the RAG post-cleavage complex *in vitro* and *in vivo*.

Our data support a common model for genomic instability in *Rag2*$^{c/c}$ *p53*$^{-/-}$ and *Atm*$^{-/-}$ mice: premature release of RAG-generated double-strand breaks from the RAG post-cleavage complex allows ends to escape the normal joining mechanisms, to persist and to be potentially joined by alternative non-homologous end joining, a pathway permissive for chromosome translocations and amplification[4,29]. Both end release and end persistence are promoted by ATM deficiency[2,3], probably because ATM both stabilizes the RAG post-cleavage complex[3] and activates p53-dependent checkpoints/apoptosis. In *Rag2*$^{c/c}$ *p53*$^{-/-}$ mice, end persistence might be augmented by ongoing RAG activity through the cell cycle resulting from impaired degradation of core RAG2, which lacks the cell-cycle-regulated degradation motif[18,30].

The complete penetrance, rapid development of lymphoma and extraordinary degree of RAG-mediated genomic instability make *Rag2*$^{c/c}$ *p53*$^{-/-}$ mice an attractive model for investigating the spectrum of somatic genome rearrangements underlying lymphomagenesis.

METHODS SUMMARY

Mice. Mice were bred in the New York University Specific Pathogen Free facility; animal care was approved by the NYU SoM Animal Care and Use Committee (protocol number 090308-2).

Analysis of tumour cells. Lymphoid tumours were analysed by flow cytometry with antibodies against surface B- and T-cell markers. Metaphases were prepared and analysed as described in Methods.

FISH and image analysis. DNA FISH was performed using BAC probes as described in Methods. Interphase FISH was performed on double-positive

thymocytes isolated by cell sorting according to protocols described in Methods. Images were obtained by confocal microscopy on a Leica SP5 AOBS system, with optical sections separated by 0.3 μm. Images were analysed using Image J software. Metaphase spreads were imaged by fluorescent microscopy on a Zeiss Imager Z2 Metasystems METAFER 3.8 system and analysed using ISIS software. Statistical analysis of image parameters used a two-tailed Fisher's exact test.

Biochemical end-release assay. The stability of RAG-signal end complexes was measured as described in Methods. Briefly, RAG cleavage reactions were divided into aliquots in microfuge tubes and incubated at the indicated temperatures for 30 min, followed by polyacrylamide gel electrophoresis. DNA was stained using SYBR Safe DNA Gel Stain (Invitrogen) and quantified with Quantity One software (Biorad). Student's *t*-test assuming equal variance was used to calculate statistical significance.

aCGH analysis. For CGH, genomic DNA from mouse thymic lymphomas was profiled against matched thymic DNA from wild-type mice. aCGH experiments were performed on two-colour Agilent 244A Mouse Genome Microarrays. Data analysis was performed as described in Methods.

Full Methods and any associated references are available in the online version of the paper at www.nature.com/nature.

Received 6 May; accepted 15 December 2010.

1. Kuppers, R. & Dalla-Favera, R. Mechanisms of chromosomal translocations in B cell lymphomas. *Oncogene* **20,** 5580–5594 (2001).
2. Callen, E. *et al.* ATM prevents the persistence and propagation of chromosome breaks in lymphocytes. *Cell* **130,** 63–75 (2007).
3. Bredemeyer, A. L. *et al.* ATM stabilizes DNA double-strand-break complexes during V(D)J recombination. *Nature* **442,** 466–470 (2006).
4. Zhu, C. *et al.* Unrepaired DNA breaks in p53-deficient cells lead to oncogenic gene amplification subsequent to translocations. *Cell* **109,** 811–821 (2002).
5. Gao, Y. *et al.* Interplay of p53 and DNA-repair protein XRCC4 in tumorigenesis, genomic stability and development. *Nature* **404,** 897–900 (2000).
6. Difilippantonio, M. J. *et al.* DNA repair protein Ku80 suppresses chromosomal aberrations and malignant transformation. *Nature* **404,** 510–514 (2000).
7. Zha, S. *et al.* ATM-deficient thymic lymphoma is associated with aberrant tcrd rearrangement and gene amplification. *J. Exp. Med.* **207,** 1369–1380 (2010).
8. Callen, E. *et al.* Chimeric IgH-TCRα/δ translocations in T lymphocytes mediated by RAG. *Cell Cycle* **8,** 2408–2412 (2009).
9. Matei, I. R. *et al.* ATM deficiency disrupts *Tcra* locus integrity and the maturation of CD4+CD8+ thymocytes. *Blood* **109,** 1887–1896 (2007).
10. Liyanage, M. *et al.* Abnormal rearrangement within the α/δ T-cell receptor locus in lymphomas from Atm-deficient mice. *Blood* **96,** 1940–1946 (2000).
11. Barlow, C. *et al.* Atm-deficient mice: a paradigm of ataxia telangiectasia. *Cell* **86,** 159–171 (1996).
12. Corneo, B. *et al.* Rag mutations reveal robust alternative end joining. *Nature* **449,** 483–486 (2007).
13. Lee, G. S., Neiditch, M. B., Salus, S. S. & Roth, D. B. RAG proteins shepherd double-strand breaks to a specific pathway, suppressing error-prone repair, but RAG nicking initiates homologous recombination. *Cell* **117,** 171–184 (2004).
14. Jones, J. M. & Simkus, C. The roles of the RAG1 and RAG2 "non-core" regions in V(D)J recombination and lymphocyte development. *Arch. Immunol. Ther. Exp. (Warsz.)* **57,** 105–116 (2009).
15. Liang, H. E. *et al.* The "dispensable" portion of RAG2 is necessary for efficient V-to-DJ rearrangement during B and T cell development. *Immunity* **17,** 639–651 (2002).
16. Qiu, J. X., Kale, S. B., Yarnell Schultz, H. & Roth, D. B. Separation-of-function mutants reveal critical roles for RAG2 in both the cleavage and joining steps of V(D)J recombination. *Mol. Cell* **7,** 77–87 (2001).
17. Steen, S. B., Han, J.-O., Mundy, C., Oettinger, M. A. & Roth, D. B. Roles of the "dispensable" portions of RAG-1 and RAG-2 in V(D)J recombination. *Mol. Cell. Biol.* **19,** 3010–3017 (1999).
18. Curry, J. D. & Schlissel, M. S. RAG2's non-core domain contributes to the ordered regulation of V(D)J recombination. *Nucleic Acids Res.* **36,** 5750–5762 (2008).
19. Talukder, S. R., Dudley, D. D., Alt, F. W., Takahama, Y. & Akamatsu, Y. Increased frequency of aberrant V(D)J recombination products in core RAG-expressing mice. *Nucleic Acids Res.* **32,** 4539–4549 (2004).
20. Jacks, T. *et al.* Tumor spectrum analysis in p53-mutant mice. *Curr. Biol.* **4,** 1–7 (1994).
21. Liao, M. J. *et al.* No requirement for V(D)J recombination in p53-deficient thymic lymphoma. *Mol. Cell. Biol.* **18,** 3495–3501 (1998).
22. Forster, A., Hobart, M., Hengartner, H. & Rabbitts, T. H. An immunoglobulin heavy-chain gene is altered in two T-cell clones. *Nature* **286,** 897–899 (1980).
23. Haines, B. B. *et al.* Block of T cell development in P53-deficient mice accelerates development of lymphomas with characteristic RAG-dependent cytogenetic alterations. *Cancer Cell* **9,** 109–120 (2006).
24. Dudley, D. D. *et al.* Impaired V(D)J recombination and lymphocyte development in core RAG1-expressing mice. *J. Exp. Med.* **198,** 1439–1450 (2003).
25. Difilippantonio, S. *et al.* 53BP1 facilitates long-range DNA end-joining during V(D)J recombination. *Nature* **456,** 529–533 (2008).
26. Arnal, S. M., Holub, A. J., Salus, S. S. & Roth, D. B. Non-consensus heptamer sequences destabilize the RAG post-cleavage complex, making ends available to alternative DNA repair pathways. *Nucleic Acids Res.* **38,** 2944–2954 (2010).
27. Helmink, B. A. *et al.* MRN complex function in the repair of chromosomal Rag-mediated DNA double-strand breaks. *J. Exp. Med.* **206,** 669–679 (2009).
28. Deriano, L., Stracker, T. H., Baker, A., Petrini, J. H. & Roth, D. B. Roles for NBS1 in alternative nonhomologous end-joining of V(D)J recombination intermediates. *Mol. Cell* **34,** 13–25 (2009).
29. Simsek, D. & Jasin, M. Alternative end-joining is suppressed by the canonical NHEJ component Xrcc4-ligase IV during chromosomal translocation formation. *Nature Struct. Mol. Biol.* **17,** 410–416 (2010).
30. Li, Z., Dordai, D. I., Lee, J. & Desiderio, S. A conserved degradation signal regulates RAG-2 accumulation during cell division and links V(D)J recombination to the cell cycle. *Immunity* **5,** 575–589 (1996).

Supplementary Information is linked to the online version of the paper at www.nature.com/nature.

Acknowledgements We thank M. Schlissel for the gift of *core Rag2* mice, F. Alt for the gift of *core Rag1* mice and S. Hewitt for the *Igh* BAC probes. D.B.R. was supported by National Institutes of Health Roadmap Initiative in Nanomedicine through a Nanomedicine Development Center award (1PN2EY018244), a National Institutes of Health grant CA104588 and the Irene Diamond Fund. L.D. is a Fellow of The Leukemia and Lymphoma Society. A.V.A. was supported in part by grant 1UL1RR029893 from the National Center for Research Resources, National Institutes of Health. J.A.S. was supported by a National Institutes of Health grant R01GM086852, a National Institutes of Health Challenge grant NCI R01CA145746-01, a Leukemia and Lymphoma Scholar Award and a Wellcome trust project grant 085096.

Author Contributions L.D. and D.B.R. conceived the study and co-wrote the manuscript. L.D. designed the experiments. L.D., J.C., M.C. and A.M. performed the experiments. Y.C. provided assistance with the mouse colonies. A.V.A. performed the aCGH data analysis. J.A.S. and S.C. provided technical and conceptual support. J.C. and J.A.S revised the manuscript. All the authors read and approved the manuscript.

Author Information Reprints and permissions information is available at www.nature.com/reprints. The authors declare no competing financial interests. Readers are welcome to comment on the online version of this article at www.nature.com/nature. Correspondence and requests for materials should be addressed to D.B.R. (david.roth@nyumc.org).

METHODS

Mice. We obtained wild type (Taconic), *Rag2*$^{c/c15}$, *Rag1*$^{c/c24}$, *p53*$^{-/-}$ (Jackson laboratory[20]) and *Atm*$^{-/-}$ (Jackson laboratory[11]) mice for this study. *Rag2*$^{c/c}$ or *Rag1*$^{c/c}$ mice were bred with p53-deficient mice to generate doubly deficient mice. Genotyping of these mutants was performed by PCR of tail DNA as described in the relevant references[11,15,20,24].

Characterization of tumour cells and metaphase preparation. Lymphoid tumours were analysed by flow cytometry with antibodies against surface B-cell (CD43, B220, IgM) and T-cell (CD4, CD8, CD3, TCR-β) markers. FACS analysis used a BD LSRII flow cytometer (BD Biosciences) equipped with FacsDiVa and FlowJo. For metaphase preparation, tumour cells were prepared as previously described[31,32]. Briefly, primary tumour cells were grown in complete RPMI media for 4 h and exposed to colcemid (0.04 μg ml^{-1}, GIBCO, KaryoMAX Colcemid Solution) for 2 hours at 37 °C. Then, cells were incubated in KCl 75 mM for 15 min at 37 °C, fixed in fixative solution (75% methanol/25% acetic acid) and washed three times in the fixative. Cell suspension was dropped onto pre-chilled glass slides and air-dried for further analysis.

G-banding and spectral karyotyping. Optimally aged slides were treated for the induction of G-banding following the routine procedure[33]. Spectral karyotyping was performed using the mouse chromosome SKY probe Applied Spectral Imaging according to the manufacturer's instructions to determine chromosomal rearrangements in the tumour samples. The slides were analysed using a Nikon Eclipse 80i microscope. G-banding as well as SKY images were captured and karyotyped using an Applied Spectral Imaging system.

DNA FISH probes. BAC probes for the *Igh* and *Tcrα/δ* loci were labelled by nick-translation and prepared as previously described[34,35]. For the *Igh* locus, BAC 199 (*Igh C*) and BAC RP24-386J17 (*Igh V*) were labelled in Alexa Fluor 594 and 488 respectively (Molecular Probes). For the *Tcrα/δ* locus, BAC RP23-304L21 (*Tcrα/δ V*) and RP-23 255N13 (*Tcrα/δ C*) were labelled in Alexa Fluor 488 or 594. StarFISH-concentrated mouse FITC or Cy3 chromosome 12 or 14 paints were prepared following supplier's instructions (Cambio). BAC probes were re-suspended in hybridization buffer (10% dextran sulphate, 5× Denharts solution, 50% formamide) or in paint hyb buffer, denatured for 5 min at 95 °C and pre-annealed for 45 min at 37 °C before hybridization on cells.

DNA FISH on metaphase spreads. Slides were dehydrated in ethanol series, denatured in 70% formamide / 2× SSC (pH 7–7.4) for 1 min 30 s at 75 °C, dehydrated again in cold ethanol series, and hybridized with probes o/n at 37 °C in a humid chamber. Slides were then washed twice in 50% formamide / 2× SSC and twice in 2× SSC for 5 min at 37 °C each. Finally, cells were mounted in ProLong Gold (Invitrogen) containing 4′,6-diamidino-2-phenylindole (DAPI) to counterstain total DNA.

DNA FISH on interphase nuclei. Double-positive thymocytes were isolated from total thymi on a Beckman-Coulter MoFlo cell sorter as Thy1.2^{+}CD4^{+}CD8^{+} cells using the following antibodies: PE-Cy7-coupled anti-CD90.2 (Thy1.2; 53-2.1), APC-coupled anti-CD4 (L3T4) and FITC-coupled anti-CD8 (53-6.7). Cells were washed two times in 1× PBS and dropped onto poly-L-lysine-coated coverslips. For three-dimensional DNA FISH analyses, we used a protocol for immunofluorescence / DNA FISH previously described[34,35], with protein detection step omitted. Briefly, cells were fixed in 2% paraformaldehyde / 1× PBS for 10 min at room temperature, permeabilized in 0.4% Triton / 1× PBS for 5 min on ice, incubated with 0.01 mg ml^{-1} Rnase A for 1 h at 37 °C and permeabilized again in 0.7% Triton / 0.1M HCl for 10 min on ice. Cells were then denatured in 1.9 M HCl for 30 min at room temperature, rinsed in cold 1× PBS and hybridized overnight with probes at 37 °C in a humid chamber. Cells were then rinsed in 2× SSC at 37 °C, 2× SCC at room temperature and 1× SSC at RT, 30 min each. Finally, cells were mounted in ProLong Gold (Invitrogen) containing DAPI to counterstain total DNA.

Biochemical end-release assay. End-release assay to measure the stability of the signal-end complexes was performed as previously described[26]. For RAG-mediated cleavage, 100 ng of recombination substrate (PCR product from pJH289) was incubated for 3 h at 37 °C with 200 ng purified RAG protein and 200 ng of purified recombinant HMGB1 in a buffer containing 50 mM HEPES (pH 8.0), 25 mM KCl, 4 mM NaCl, 1 mM DTT, 0.1 mg BSA, 5 mM $CaCl_2$ and 5 mM $MgCl_2$. Reactions were then divided into aliquots in microfuge tubes and incubated at different temperatures, or treated with stop buffer (10 mM Tris (pH 8.0), 10 mM EDTA, 0.2% SDS, 0.35 mg ml^{-1} proteinase K (Sigma Aldrich)) for 30 min and then run out on 4–20% acrylamide tris-borate-EDTA (TBE) gels (Invitrogen).

aCGH analysis. aCGH experiments were performed on two-colour Agilent 244A Mouse Genome Microarray. After internal Agilent quality control, the collected data were background subtracted and normalized using the Loess method[36]. We used circular binary segmentation method to define regions of copy number alteration compared with the control[37] and applied the cghMCR method for extraction of altered minimum common regions between the samples[38]. The analyses and visualizations were performed using the R statistical program[39].

31. Theunissen, J. W. & Petrini, J. H. Methods for studying the cellular response to DNA damage: influence of the Mre11 complex on chromosome metabolism. *Methods Enzymol.* **409,** 251–284 (2006).
32. Multani, A. S. *et al.* Caspase-dependent apoptosis induced by telomere cleavage and TRF2 loss. *Neoplasia* **2,** 339–345 (2000).
33. Pathak, S. Chromosome banding techniques. *J. Reprod. Med.* **17,** 25–28 (1976).
34. Hewitt, S. L. *et al.* RAG-1 and ATM coordinate monoallelic recombination and nuclear positioning of immunoglobulin loci. *Nature Immunol.* **10,** 655–664 (2009).
35. Skok, J. A. *et al.* Reversible contraction by looping of the Tcra and Tcrb loci in rearranging thymocytes. *Nature Immunol.* **8,** 378–387 (2007).
36. Yang, Y. H. *et al.* Normalization for cDNA microarray data: a robust composite method addressing single and multiple slide systematic variation. *Nucleic Acids Res.* **30,** e15 (2002).
37. Olshen, A. B., Venkatraman, E. S., Lucito, R. & Wigler, M. Circular binary segmentation for the analysis of array-based DNA copy number data. *Biostatistics* **5,** 557–572 (2004).
38. Aguirre, A. J. *et al.* High-resolution characterization of the pancreatic adenocarcinoma genome. *Proc. Natl Acad. Sci. USA* **101,** 9067–9072 (2004).
39. R. development Core Team. *R: A Language and Environment for Statistical Computing.* Vienna: R Foundation for Statistical Computing (2006).